AUTOMATIC BONE SEGMENTATION IN ULTRASOUND USING COMBINED STRAIN IMAGING AND ENVELOPE SIGNAL POWER

Mohammad Arafat Hussain MSc[1]*, Pierre Guy MD, MBA[2], Antony J. Hodgson PhD[3], Rafeef Abugharbieh PhD[1]

[1,*]Department of Electrical and Computer Engineering, University of British Columbia, Vancouver, V6T 1Z4, Canada, arafat@ece.ubc.ca

[2]Department of Orthopaedics, University of British Columbia, Vancouver, V5Z 1M9, Canada

[3]Department of Mechanical Engineering, University of British Columbia, Vancouver, V6T 1Z4, Canada

INTRODUCTION

In computer assisted orthopaedic surgery (CAOS), fluoroscopy remains the primary intraoperative imaging modality for bone boundary visualization. However, the associated radiation exposure poses risks to both patients and surgical teams. Ultrasound (US) imaging has thus recently emerged as a safer (non-ionizing) potential alternative intraoperative imaging modality; in recent years, our group has introduced and evaluated a set of techniques based on phase symmetry processing for accurately identifying bone surfaces in 2D and 3D ultrasound images (Hacihaliloglu 2011, 2012, 2014, Brounstein, 2011).

Previous automatic bone segmentation methods in US based on image intensity and local gradient (Kowal 2007, Patwardhan 2012) had difficulties dealing with the high level of speckle noise, reverberation, anisotropy, and signal dropout that is typical in US data. Local image phase feature-based bone segmentation methods (Hacihaliloglu 2008) addressed some of these limitations, though situations can arise in which there can be false positive bone responses at soft tissue interfaces that exhibit similar intensity profiles as bone interfaces.

To reduce the potential for such false positives, we present here a method for automatic bone segmentation that is based on combining US strain imaging (i.e., elastography) and the envelope power signal. Because elastography estimates tissue stiffness, we can achieve a marked reduction in false positive responses at soft tissue interfaces. In a recent preliminary study (Hussain 2014), we investigated the potential of US strain imaging and envelope power together to delineate bone boundary in US images. In this paper, we introduce enhancements such as an automatic weight selection process for fusing the strain and envelope power map based on an echo de-correlation measure between pre- and post-compression RF frames. We also deploy a local statistics-based bone discontinuity detection scheme. Further, we introduce Gaussian mixture regression (GMR) that better preserves curvature features in the bone boundary. The performance of our enhanced bone segmentation method is evaluated on a finite-element-model (FEM) phantom as well as *in vivo* data.

MATERIALS AND METHODS

Materials

FEM Simulation Phantom. We built a $40mm \times 40mm$ FEM phantom using the ANSYS analysis software (ANSYS, Inc., Canonsburg, PA) and simulated an US scan of the model using Field II (Jensen 1996). Our phantom mimicked a fractured human distal radius bone with a total number of nodes of 55,180. The stiffness of the homogeneous soft tissue and bone region were set to 10kPa and 10GPa, respectively, as previously reported in the

literature (Pistoia 2012). Our phantom was compressed from the top using a planar compressor that was wider than the phantom. An ultrasonic transducer of center frequency f_o= 5MHz and bandwidth = 50% was used to simulate the phantom scan from the top. The total number of scan-lines was 128. We set an applied pressure level that corresponds to a 1% average strain. We did not model out-of-plane motion.

In Vivo Data. We acquired three sets of *in vivo* US data with free-hand compression from three volunteers (volunteer-I: 25-year old male; volunteer-II: 33-year old male; volunteer-III: 26-year old male) after proper prior consent was obtained. US data were acquired using a SonixRP scanner integrated with an L14-5W/60 probe operating at 10MHz.

Method

Strain and Envelope Power Map Fusion. To efficiently segment bone in the US image, we fused a modified strain (MSM) and envelope power map (MEM) of the region-of-interest (ROI) (Hussain 2014) as $FM = \lambda \times MSM + (1 - \lambda) \times MEM$, where λ is a weighting parameter and FM is the fused map. In our previous work, we empirically chose $\lambda = 0.5$ (Hussain 2014). To automate the selection of λ, in this work we incorporate the echo de-correlation measure between the pre- and post-compression RF frames. Freehand elastography is prone to echo de-correlation and with an increase in applied pressure, echo de-correlation increases significantly leading to noisy strain maps (Hussain 2012). A noisy strain map may significantly deteriorate the bone boundary localization accuracy. Therefore, we choose the value for λ inversely proportional to the echo de-correlation present in the elastographic data which ultimately controls the contribution of the MSM into the FM.

To measure the degree of echo de-correlation, we estimate an average normalized cross-correlation (NCC) peak ρ_{avg} between pre- and post-compression RF windows for a Region of Interest (ROI) near the transducer face. We consider three cases: (1) if ρ_{avg} is greater than 0.9, this indicates good correlation between the pre- and post-compression RF frames (Zahiri-Azar 2006). In that case, we use $\lambda = 0.5$ since our FEM phantom study indicates this value to be the optimum. (2) If ρ_{avg} is less than 0.5 (while NCC coefficients are in the range from 0 to 1), then it is obvious that the degree of de-correlation is greater than the correlation (Zahiri-Azar 2006). In that case, we use $\lambda = 0$. And (3) if ρ_{avg} varies between 0.9 and 0.5, we assume a linear relation of λ with ρ_{avg} and thus choose the value for λ from a linear function defined as

$$\lambda = \frac{5}{4}(\rho_{avg} - 0.5). \tag{1}$$

The location of maximum intensity point along each scan-line is then used as the initial bone boundary $Y (= [y_1, y_2, \ldots . y_n])$, where y_i is the axial sample number at ith scan-line in the fused map and n is the total number of scan-lines.

Bone Discontinuity Detection. To detect possible discontinuity in the bone surface, we estimate the gradient $\frac{dY}{dX} = \nabla Y$ after linear regression, where $X (= x_a|_{a=1\ldots n})$ is the lateral sample number in the fused map. Then we use the local statistics of ∇Y such that any point on ∇Y exceeds $\mu + 3\sigma$ (where μ and σ are the mean and standard deviation of ∇Y, respectively) is flagged as a bone discontinuity. We choose $\mu + 3\sigma$ to cover a confidence interval of 0.997 assuming that ∇Y is normally distributed. Each continuous portion of Y is considered a segment and after finding all the segments, we use Gaussian mixture regression (GMR) over each of the segments separately, in contrast to our previous work (Hussain 2014) where we

used linear regression over $\boldsymbol{Y}$, which cannot model generally nonlinear patterns in data space (e.g. curved bone).

Gaussian Mixture Regression. In this work, we use GMR that overcomes the following drawbacks of linear regression which we used in our previous work (Hussain 2014):

1. Choosing a suitable length for regression window is ambiguous since smaller windows cannot produce smoother bone boundary if $\boldsymbol{Y}$ is noisy. On the other hand, comparatively larger regression window causes loss of local curvature information in $\boldsymbol{Y}$.

2. Parametric linear regression models are often too rigid to model general nonlinear patterns in data space and thus, a more flexible model of non-parametric regression is required (Sung 2004).

Now $f_{X,Y}(x,y) = \sum_{j=1}^{K} \pi_j \emptyset(x,y;\mu_j,\Sigma_j)$ be the joint density function of bone indicating points in the fused map, where K is the total number of clusters present in $\boldsymbol{Y}$ which is estimated from spectral clustering (Zelnik-Manor 2004), π_j, $\mu_j = \begin{bmatrix} \mu_{jX} \\ \mu_{jY} \end{bmatrix}$ and $\Sigma_j = \begin{bmatrix} \Sigma_{jX} & \Sigma_{jXY} \\ \Sigma_{jYX} & \Sigma_{jYY} \end{bmatrix}$ are the probability, mean and covariance matrix, respectively, of the data points in jth cluster and are estimated from an expectation maximization algorithm (Cohn 1996), and $\emptyset(x,y;\mu_j,\Sigma_j)$ is the probability density function of points inside jth cluster defined as

$$\emptyset(x,y;\mu_j,\Sigma_j) = \frac{1}{2\pi\sqrt{|\Sigma_j|}} \exp[-\frac{1}{2}(D-\mu_j)^T \Sigma_j^{-1}(D-\mu_j)], \tag{2}$$

where $D = \begin{bmatrix} X \\ Y \end{bmatrix}$. Then, from the joint density function $f_{X,Y}(x,y)$, our GMR equation can be derived (Sung 2004) which takes the form as

$$m(x) = E[\boldsymbol{Y}|\boldsymbol{X}=x] = \sum_{j=1}^{K} w_j(x)d_j(x), \tag{3}$$

where $d_j(x) = \mu_{jY} + \Sigma_{jYX}\Sigma_{jX}^{-1}(x-\mu_{jX})$, and μ_{jX} and Σ_{jX} are the mean and covariance matrix of the marginal density function (f_X) of $\boldsymbol{X}$, in the jth data cluster. In addition, $w_j(x)$ is the mixing weight defined as

$$w_j(x) = \frac{\pi_j \emptyset(x;\mu_{jX},\Sigma_{jX})}{\sum_{j=1}^{K} \pi_j \emptyset(x;\mu_{jX},\Sigma_{jX})}. \tag{4}$$

RESULTS
We compare our results to those of the adaptively parameterized local phase feature-based bone segmentation presented by Hacihaliloglu (2011).

FEM Results. In Figs. 1(a), (b), (c) and (d), we show the B-mode, estimated strain, envelop power images, and fused map, respectively, for the FEM model. In Figs. 1(e) and 1(f), we show the bone boundaries detected by the proposed and APS method, respectively. The figures demonstrate that the APS method produces several false positive bone responses which led to some artifacts in the place of bone discontinuity when bottom-up ray casting is used (as suggested in Hacihaliloglu 2011). In contrast, the bone boundaries produced by our method [see Fig. 1(e)] are free of such artifacts. We also compare the quantitative

performance of the proposed and APS methods in terms of mean absolute error (MAE) (Hussain 2014) in Fig. 1(g) with four different signal-to-noise ratio (SNR) simulations (40, 30, 20, and 10dB) with 100 realizations each. We estimate the actual bone boundary from the ideal strain map that is considered ground truth. As can be seen in these figures, the APS method has a mean MAE approximately 25% greater than that of the proposed method with relatively low sensitivity to the signal-to-noise ratio (SNR).
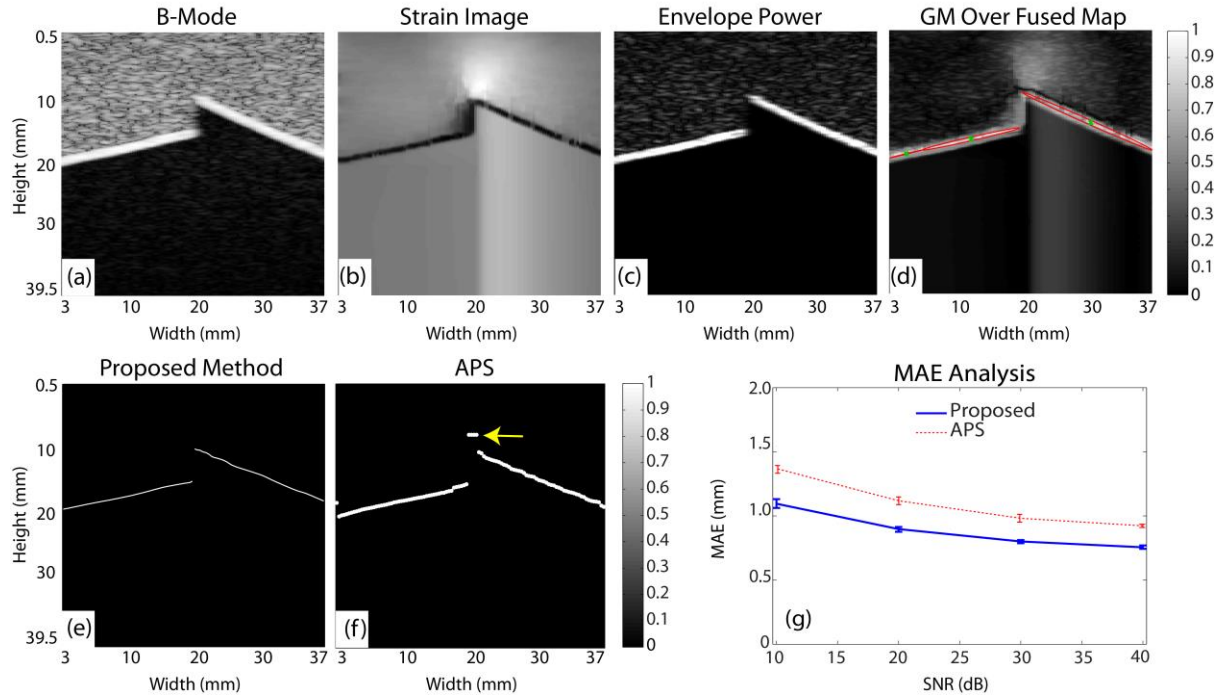

Figure 1: Illustration of bone boundary detection using the FEM phantom. (a) B-mode image, (b) strain image, (c) envelop power map, (d) Gaussian mixtures representation over fused map, (e) estimated bone boundary by the proposed method, (f) estimated bone boundary by the APS method (bone boundary is shown after bottom-up ray casting), and (g) MAE analysis of the proposed and APS methods at different SNRs.

In Vivo Results. The scanned bone regions on the anatomies as well as the B-mode images of volunteers-I, II, and III are shown in Figs. 2(a)-(c) and (m)-(o), respectively. An Orthopedic expert delineated the bone boundaries on the B-mode images [see Figs. 2(m)-(o)] which we consider as ground truths for a comparative analysis of the proposed and APS methods. In Figs. 2(d)-(f), we show the strain images. We can see from Figs. 2(m)-(o) that the bone boundary produced by the APS method varies noticeably in some places. This variation results from the false positive bone responses. In contrast, in all three cases, the bone boundaries estimated by our proposed method better match the shapes as marked by the expert in the corresponding B-mode images [see Figs. 2(m)-(o)]. In addition, our method did not produce false positives at soft tissue interfaces.

DISCUSSION

We presented a method for robust bone boundary localization based on the fusion of strain imaging and envelope signal power detection. To improve our initial approach (Hussain 2014) as well as make that bone segmentation method more robust, we have introduced a number of automation techniques in the selection of parameters. We have introduced automatic weight selection technique based on an echo de-correlation measure between the pre- and post-compression RF frames to fuse the MSM and MEM. We have also used a data-driven bone discontinuity detection scheme and introduced multivariate non-parametric Gaussian mixture regression. Our results demonstrated reduced bone localization error

through addressing the false positive bone response. We demonstrated our improved performance on two types of validation data including a simulated FEM phantom, and three sets of *in vivo* volunteer data. We also compare the results of our proposed method with that of a state-of-the-art method (Hacihaliloglu 2011). We have shown an improvements of approximately 25% in terms of MAE in the FEM simulation test, when compared with current state-of-the-art. In addition, the qualitative performance with the *in vivo* data is also found to be better for the proposed method when compared with the state-of-the-art APS method. The key limitation of the proposed strain and envelope signal power-based approach is that it is currently restricted to use with 2D images; we are therefore exploring the potential for expanding this approach for use with 3D image sets.
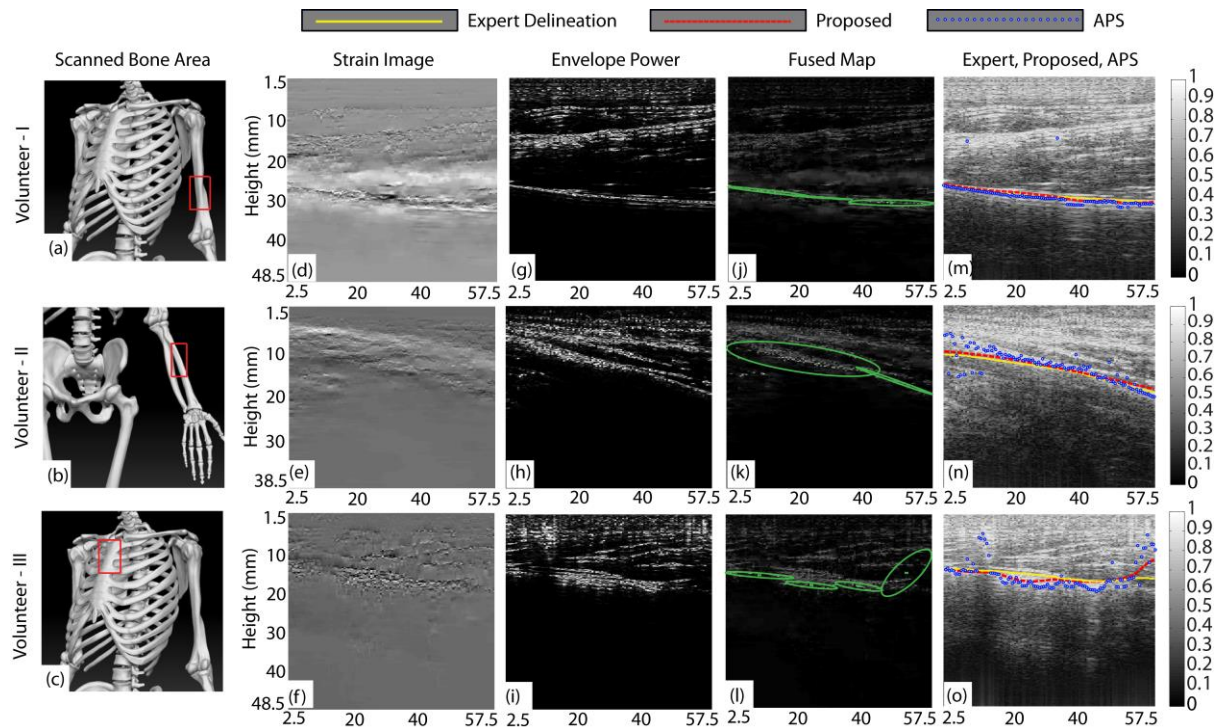

Figure 7. Illustration of the bone boundary detection using the *in vivo* data. (a)-(c) show bone regions scanned on each volunteer (with red rectangles), (d)-(f) are strain images, (g)-(i) are the envelope power maps, and (j)-(l) are the fused maps with Gaussian mixtures overlaid. Finally, in (m)-(o), orthopedic expert delineated bone boundaries, and detected bone boundaries by the APS (bone boundary is shown after bottom-up ray casting) and proposed methods are overlaid on the respective B-mode images for all the volunteers.

ACKNOWLEDGEMENTS

REFERENCES

- Hacihaliloglu I, Abugharbieh R, Hodgson AJ, Guy P, Automated Bone Contour Detection in 3D B- Mode Ultrasound Images Using Optimized Phase Symmetry Features—A Clinical Evaluation for Pelvic Fractures. In: Meeting of the International Society for Computer Assisted Orthopaedic Surgery (CAOS), London-UK, pp. 1-3, 2011.
- Hacihaliloglu I, Brounstein A, Guy P, Hodgson AJ, Abugharbieh R, 3D Ultrasound-CT Registration in Orthopaedic Trauma Using GMM Registration with Optimized Particle Simulation-Based Data Reduction, In: N. Ayache et al. (Eds.): MICCAI 2012, Part II, LNCS 7511, pp. 82–89, 2012.

- Hacihaliloglu I, Guy P, Hodgson AJ, Abugharbieh R, Volume-Specific Parameter Optimization of 3D Local Phase Features for Improved Extraction of Bone Surfaces in Ultrasound Images, International Journal of Medical Robotics and Computer Assisted Surgery, 2014.
- Brounstein A, Hacihaliloglu I, Guy P, Hodgson AJ, Abugharbieh R, Towards Real-Time 3D US to CT Bone Image Registration using Phase and Curvature Feature Based GMM Matching, In: G. Fichtinger, A. Martel, and T. Peters (Eds.): MICCAI 2011, Part I, LNCS 6891, pp. 235–242, 2011
- Hacihaliloglu I, Abugharbieh R, Hodgson AJ, Rohling RN, Bone Segmentation and Fracture Detection in Ultrasound Using 3D Local Phase Features, In: Metaxas et al. (eds.): MICCAI 2008, Part I, LNCS 5241, pp. 287–295, 2008.
- Kowal J, Amstutz C, Langlotz F, Talib H, Ballester MG, Automated Bone Contour Detection in Ultrasound B-mode Images for Minimally Invasive Registration in Computer Assisted Surgery: an In Vitro Evaluation, Int. J. Med. Robot Comput. Assist. Surg., 3(4), pp. 341–348, 2007.
- Patwardhan KA, Kunlin C, David M, Ralf T. Automated bone and joint-region segmentation in volumetric ultrasound, In *IEEE International Symposium on*, pp. 1327-1330, 2012.
- Hussain MA, Hodgson AJ, Abugharbieh R, Robust Bone Detection in Ultrasound Using Combined Strain Imaging and Envelope Signal Power Detection, In: P. Golland et al. (eds.): MICCAI 2014, Part I, LNCS 8673, pp. 356–363, 2014.
- Jensen, JA, Field: A Program for Simulating Ultrasound Systems. In: 10th Nordicbaltic Conf. on Biomed. Imag. Part I, 4(1), pp. 351–353, 1996.
- Hussain MA, Anas EMA, Alam SK, Lee SY, Hasan MK, Direct and Gradient Based Average Strain Estimation by Using Weighted Nearest Neighbor Cross-correlation Peaks, IEEE Trans. Ultra. Ferro. Freq. Cont. 59(8), pp. 1713–1728, 2012.
- Sung HG, Gaussian Mixture Regression and Classification, Ph.D. dissertation, Dept. Statis., Rice Univ., Houston, TX, 2004.
- Zelnik-Manor L, Perona P, Self-tuning Spectral Clustering, Advances in Neural Information Processing Systems 17, pp. 1601–1608, 2004.
- Cohn DA, Ghahramani Z, Jordan MI, Active Learning with Statistical Models, Jour. of Arti. Intel. Research, 4, pp. 129-145, 1996.
- Pistoia W, Rietbergen BV, Lochmuller E, Lill CA, Eckstein F, Ruegsegger PR, Estimation of Distal Radius Failure Load With Micro-Finite Element Analysis Models Based on Three-dimensional Peripheral Quantitative Computed Tomography Images," *Bone*, 30(6), pp. 842–848, 2002.
- Zahiri-Azar, R, Salcudean, SE, Motion Estimation in Ultrasound Images Using Time Domain Cross Correlation With Prior Estimates, IEEE Transactions on Biomedical Engineering, 53(10), pp. 1990-2000, 2006.
- Hacihaliloglu I, Abugharbieh R, Hodgson AJ, Rohling RN, Automatic Adaptive Parameterization in Local Phase Feature-based Bone Segmentation in Ultrasound, Ultras. in Med. and Biol., 37(10), pp. 1689–1703, 2011.